Ex vivo blood vessel imaging using ultrasound-modulated optical microscopy

Sri-Rajasekhar Kothapalli
Lihong V. Wang
Washington University in St. Louis
Department of Biomedical Engineering
Optical Imaging Laboratory
St. Louis, Missouri 63130

Abstract. Recently we developed ultrasound-modulated optical microscopy (UOM) based on a long-cavity confocal Fabry-Perot interferometer (CFPI). This interferometer is used for real-time detection of multiply scattered light modulated by high frequency (30 to 75 MHz) ultrasound pulses propagating in an optically, strongly scattering medium. In this work, we use this microscope to study the dependence of ultrasound-modulated optical signals on the optical absorption and scattering properties of objects embedded about 3 mm deep in tissue mimicking phantoms. These results demonstrate that UOM has the potential to map both optical absorption and scattering contrast. Most importantly, for the first time in the field of ultrasound-modulated optical imaging, we image blood vasculature in highly scattering tissue samples from a mouse and a rat. Therefore, UOM could be a promising tool to study the morphology of blood vasculature and blood-associated functional parameters, such as oxygen saturation. © *2009 Society of Photo-Optical Instrumentation Engineers.* [DOI: 10.1117/1.3076191]

Keywords: ultrasound-modulated optical microscopy; ultrasound; multiply scattered light; confocal Fabry-Perot interferometer; microscopy.

Paper 08379 received Oct. 20, 2008; accepted for publication Dec. 10, 2008; published online Feb. 11, 2009.

1 Introduction

Imaging of intrinsic optical contrast can reveal tissue structure, molecular-specific signaling pathways, and physiological functions of living subjects.[1–7] Hemoglobin is a widely imaged biomolecule that possesses strong optical absorption. By exploiting differential absorption at a set of suitable visible or near-infrared wavelengths, the concentrations of two forms of hemoglobin, oxyhemoglobin and deoxyhemoglobin, can be quantified. Using these concentrations, the saturation level of oxygen (SO_2), a physiologically important functional parameter, can be inferred. For example, tumor development usually involves hypoxia, a low level of SO_2. Therefore, blood vasculature and SO_2 can be readily mapped by modalities sensitive to optical absorption.[5,8–11] On the other hand, optical scattering is primarily related to structural changes at the cellular and subcellular levels. Variations in scattering can provide information about diseased tissue[8] and neuronal activity.[2,12] Therefore, it is important to image both optical absorption and optical scattering to obtain comprehensive information about biological tissue. Current optical microscopy techniques that image beyond a transport mean free path are either primarily sensitive to optical scattering (optical coherence tomography) or optical absorption (photoacoustic microscopy). It remains a challenge to provide both optical absorption and scattering contrasts using a single microscopy technique. In this work, we not only demonstrate that ultrasound-modulated optical microscopy (UOM) can provide both optical absorption and scattering contrasts, but also explore the feasibility of UOM for imaging intrinsic optical properties of biological tissue.

Optical imaging offers excellent intrinsic optical contrast, but suffers from poor spatial resolution at depths beyond one transport mean free path in biological tissue due to strong scattering of light in biological tissue. On the other hand, ultrasound imaging offers excellent spatial resolution and imaging depth, both of which are scalable with ultrasound parameters. However, it provides poor contrast for soft tissue imaging. Ultrasound-modulated optical imaging is a promising hybrid imaging modality that combines the advantages of both ultrasound and optical imaging.[11,13] It uses a focused ultrasound wave to modulate multiply scattered light inside the biological tissue. The detected modulated light is more sensitive than the measured nonmodulated light intensity to the local optical properties of the tissue within the ultrasound beam.[14] Therefore, this imaging modality combines ultrasonic resolution and optical contrast. Moreover, mechanical contrast of soft biological tissue can also be imaged by time gating the modulated light.[15] The physical mechanism of the modulation can be attributed to ultrasound-induced displacements of optical scatterers and to ultrasound-induced changes in the optical index of refraction.[16–19] Since ultrasound waves consist of both compressions and rarefactions, each scattered photon passing through the ultrasound column acquires positive and negative phase shifts. Therefore, the net phase accumulation along the total path length is relatively small. Moreover, the volume occupied by ultrasound inside the tissue is much smaller than the volume occupied by multiply scattered photons. Thus the volume of ultrasound and light interaction is

Address all correspondence to: Lihong V. Wang, Optical Imaging Laboratory, Department of Biomedical Engineering, Washington University of St. Louis, St. Louis, Missouri 63130. E-mail: lhwang@biomed.wustl.edu.

1083-3668/2009/14(1)/014015/6/$25.00 © 2009 SPIE

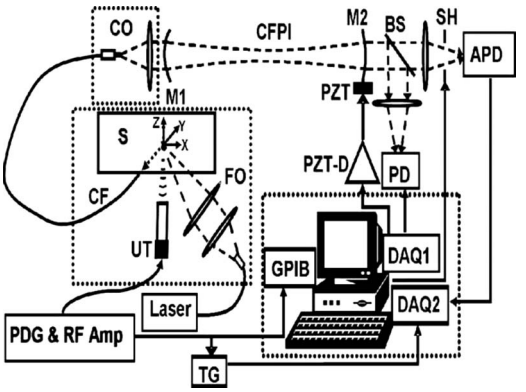

Fig. 1 (a) Schematic of the experimental setup: APD, avalanche photodiode; BS, beamsplitter; CF, collecting fiber; CFPI, confocal Fabry-Perot interferometer; CO, coupling optics; DAQ, data acquisition board; FO, focusing optics; M1 and M2, mirrors inside the cavity; PD, photodetector; PDG, pulse delay generator; PZT, piezoelectric transducer; PZT-D, piezoelectric transducer driver; RF Amp, RF amplifier; S, sample; SH, shutter; TG, trigger generator; and UT, ultrasonic transducer.

relatively small compared to that of the nonmodulated light. Consequently, various detection schemes have been proposed to detect ultrasound-modulated light efficiently.[12,20–28] At present, detection schemes based on photorefractive crystals,[25,28] Fabry-Perot interferometers,[26,29] and hole-burning crystals[27] are the most suitable choices for fast parallel speckle detection. Recently we developed ultrasound-modulated optical microscopy (UOM) based on the confocal Fabry-Perot interferometer (CFPI) detection scheme.[29] UOM can provide micron-scale resolution and high optical contrast images of scattering biological tissue at imaging depths beyond 2 mm.

We use UOM to first study the dependence of ultrasound-modulated optical signals on the optical absorption and the scattering properties of objects embedded about 3 mm deep inside tissue mimicking phantoms. Our results demonstrate that UOM can provide both optical absorption and scattering contrasts. Further, our results on absorbing objects show that the image contrast of absorbing objects is nearly linearly proportional to the absorption coefficient of the object. Most importantly, we use this microscope to image intact blood vessels in tissue (such as ear and skin) samples of a mouse and a rat. Our B-scan results show that images can be formed of the interior of blood vessels. Further, we use maximum intensity projection (MIP)[30] along the axial (depth) direction and succeed in showing the structure of blood vessels. In the field of ultrasound-modulated optical imaging, for the first time, we report imaging using intrinsic optical contrast (absorption due to blood), which is essential for functional imaging of biological tissue.

2 Experimental Methods

2.1 *Experimental Setup*

The details of the UOM experimental setup (Fig. 1) based on CFPI (50-cm cavity length, 0.1-mm^2 sr etendue, and ~20 finesse) have been described earlier. The CFPI is used as a real-time optical filter for filtering multiply scattered light modulated by high frequency ultrasound pulses propagating in biological tissue. Figure 1 shows the configuration of the sample S that is imaged, as well as the oblique configuration of the light illumination and ultrasound insonification of the sample S. The axis of propagation of the ultrasonic beam is along the z axis. The light beam propagates about 35 deg with respect to the ultrasonic beam. The ultrasonic and optical beams were focused to the same spot below the sample surface. We used a high frequency focused ultrasound transducer with a central frequency of 30 MHz (Panametrics, 4.25-μs fused silica delay lines, 6.35-mm element sizes, 5.5-mm focal lengths, and 80% estimated fractional bandwidths). This focused transducer is modified from a commercial broadband delay-line transducer (V213-BB-RM, Panametrics, Waltham, Massachusetts) by grinding a concave spherical lens directly in its quartz delay line. This concave lens works as a focusing acoustic lens. The lateral resolution of UOM in biological tissues is mainly determined by the center frequency and the numerical aperture (NA) of the ultrasound transducer, and the axial resolution is primarily determined by the frequency bandwidth of the ultrasound transducer. The center frequency also limits the imaging depth due to the frequency-dependent ultrasonic attenuation, 0.7–3 dB/(cm.MHz) in human skin. Our earlier experiments, using an ultrasound transducer with a 30-MHz central frequency, showed that an axial resolution of about 60 μm and a lateral resolution of 70 μm could be achieved in a depth range of about 2.5 mm in chicken breast tissue.[29] As in the earlier work, in these experiments the transducer was driven by a square bipolar pulse with a period of 34 ns. This bipolar pulse was generated by a trigger generator (DG535 Stanford Research, Sunnyvale, California) and amplified (Amplifier Research, 75A250). The focal ultrasound pressure measured by a needle hydrophone (ONDA HNV-0200) was about 3 MPa, within the ultrasound safety limit at these frequencies for tissues without well-defined gas bodies.[31]

In this experiment, the laser light (Coherent, Verdi, 532-nm wavelength) was focused onto a spot ~100 μm in diameter below the surface of an otherwise scattering-free sample. The optical power delivered to the sample was about 50 mW. However, for *in vivo* experiments, the duration of the light exposure to the living subject could be reduced to only a few μs for each cycle of ultrasound propagation through the region of interest, to meet the ANSI safety limit for average power.[32] Diffusely reflected light was collected by a multimode optical fiber with a 600-μm core diameter. The sample was mounted on a three-axis motorized translational stage and controlled by the LabView program. The ultrasound transducer (UT) and the sample S were immersed in water for acoustic coupling, and thus the light focusing optics (FO) and the collecting fiber (CF) were also immersed in the same water tank. The collected light was coupled into the CFPI using coupling optics (CO), and was operated in transmission mode. Details about the subsequent ultrasound-modulated optical signal detection using the CFPI were discussed in our earlier work.[29] The photodiode (PD) (New Focus, model 2031, New Focus, San Jose, California) was used in a cavity alignment procedure. The signal acquired by an avalanche photodiode (APD, Advanced Photonix, Ann Arbor, Michigan) during the ultrasound propagation through the sample represented the

distribution of the ultrasound-modulated optical intensity along the ultrasonic axis. Therefore, it yielded a 1-D image (A-line) along the z direction. In each operational cycle, the resonant frequency of the CFPI was tuned first, and then data from 4000 ultrasound pulses were acquired in one second. Averaging of 3 to 5 cycles was usually needed to obtain a satisfactory signal-to-noise ratio (SNR) for each 1-D image. 2-D images were obtained by scanning the sample along the z direction and acquiring each corresponding 1-D image.

After each B-scan along the x axis, the sample was returned to its original x coordinate and further translated by one scanning step (usually 0.1 mm) along the y axis to start a new B-scan. Thus several B-scans were obtained by raster scanning the sample in the x-y plane. To obtain high contrast blood vessel imaging, each B-scan was processed by subtracting each A-line in the B-scan from an A-line obtained from the transparent region of the respective B-scan. We further performed maximum intensity projection (MIP) on each of the processed B-scan images along the z axis. The final MIP image was obtained by combining projections from all B-scans.

2.2 *Phantom Preparation*

Ultrasound-modulated optical imaging is primarily aimed at imaging intrinsic optical contrast of soft biological tissue. Therefore, we prepared several objects of different absorption coefficients (including a nearly transparent object), and measured the ultrasound-modulated optical signal with our UOM setup, presented in Fig. 1. The four objects were made of 15% porcine gelatin, with different amounts of Trypan Blue dye, so that the optical absorption coefficients at 532 nm were 145, 72, 36, and 0.1 cm^{-1} (whole blood absorption at 532 nm is around 120 cm^{-1}). The approximate dimensions of all four objects were 1, 2, and 1 mm in the x, y, and z directions. These objects were transparent enough for the ultrasound and absorptive for the light. The background tissue phantom was made from gelatin, water, and 1% Intralipid (20% Liposyn II, Intravenous Fat Emulsion Hospira, Incorporated, Lake Forest, Illinois) with a 1-mm optical transport mean free path. The tissue phantom was an optically scattering slab 10 cm wide in the x and y axes (the ultrasound scanning axes, or the B-scan and C-scan directions, respectively) and 5 mm thick in the z axis (ultrasound propagation direction). The optical reduced scattering and absorption coefficients of the scattering slab (background medium) were $\mu_s'=10$ cm^{-1} and $\mu_a=0.1$ cm^{-1}, respectively. As shown in Fig. 2(a), a piece of stainless steel needle (254-μm outer diameter) and all four objects were placed inside the scattering slab at a depth of $z=3$ mm. Figure 2(b) shows a photograph of the prepared phantom. Since ultrasound waves were strongly reflected by the needle, it helped in aligning all four objects precisely at the ultrasound focal point. We used a pulser (GE Panametrics, 5072PR) in this alignment procedure.

We obtained several ear and skin tissue samples from a mouse and a rat sacrificed during other experiments in our laboratory. As shown in Figs. 3(a) and 4(a), a piece of stainless steel needle (254-μm outer diameter) and these tissue samples were then placed inside an optically clear medium (made from gelatin and water) at a depth of $z=2.5$ mm (the ultrasound propagation direction). This clear medium was

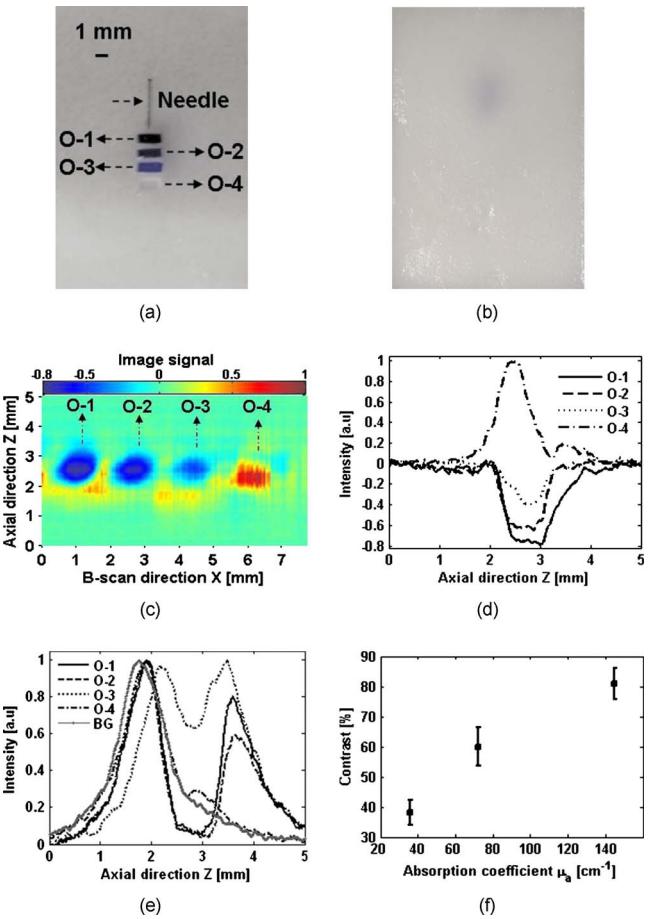

Fig. 2 Dependence of ultrasound-modulated optical signal on optical properties. (a) Photograph of three optically absorbing objects (μ_a =145 cm^{-1}, μ_a=72 cm^{-1}, μ_a=36 cm^{-1}, and all three having the same μ_s'=0.5 cm^{-1}) and one transparent object (μ_a=0.1 cm^{-1}, μ_s' =0.5 cm^{-1}) placed vertically below a piece of needle, respectively. These four objects are marked as O-1, O-2, O-3, and O-4, respectively. (b) Photograph of the prepared phantom sample. (c) Background subtracted B-scan UOM image of the sample shown in (a). (d) Respective 1-D profiles (A-lines) along the z axis through the center of all four objects. (e) Normalized A-lines, acquired from the original (not background subtracted) data, through the centers of all four objects and the background medium BG. (f) Plot of maximum contrast of all three absorbing objects.

10 cm wide in the x and y axes (the ultrasound scanning axes, or the B-scan and C-scan directions, respectively) and 5 mm thick in the z direction.

3 Results and Discussion

3.1 *Ultrasound-Modulated Optical Signal Dependence on Optical Properties*

The contrast in ultrasound-modulated optical imaging is primarily based on optical properties of the biological tissue. Although both scattering and absorption influence the strength of the signal, variations of the ultrasound-modulated intensity are more sensitive to absorption.[33] Therefore, it is of primary importance to explore the dependence of the ultrasound-modulated optical signal on optical properties using the UOM system shown in Fig. 1. As described in the previous section,

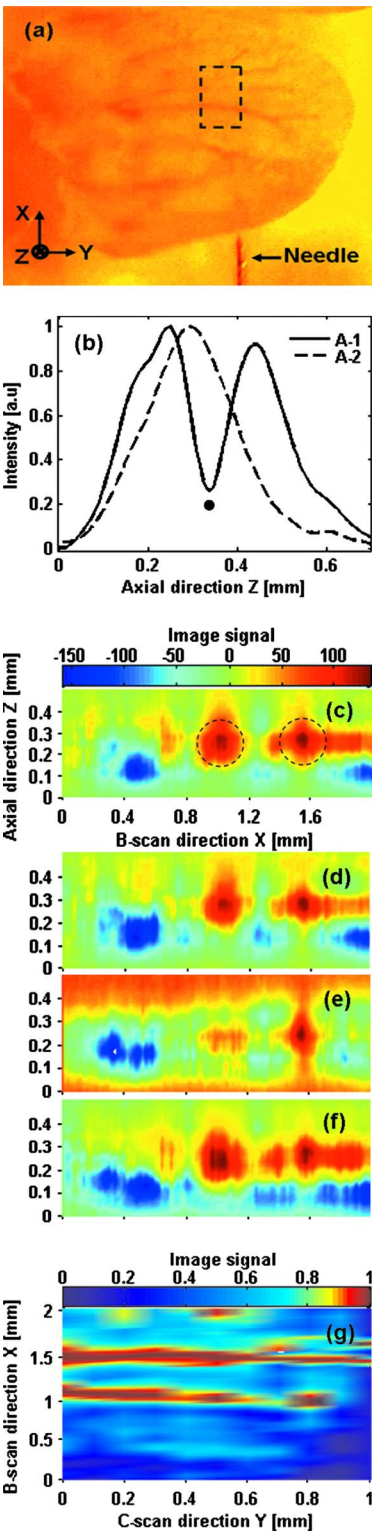

Fig. 3 Imaging intact blood vasculature in a rat ear. (a) Photograph of blood vasculature inside the rat ear. (b) A-line, A-1, represents temporal dependence of ultrasound-modulated light intensity during the propagation of ultrasound pulse through the ear tissue sample. A dot placed below this curve in the figure represents the position of the blood vessel along the ultrasound propagation direction. A-2 represents a typical A-line not passing through the blood vessel. (c) through (f) Four consecutive B-scan images that were obtained 0.2 mm apart laterally at y=0.2 mm, y=0.4 mm, y=0.6 mm, and y=0.8 mm, respectively. (g) MIP image of (a) obtained using UOM.

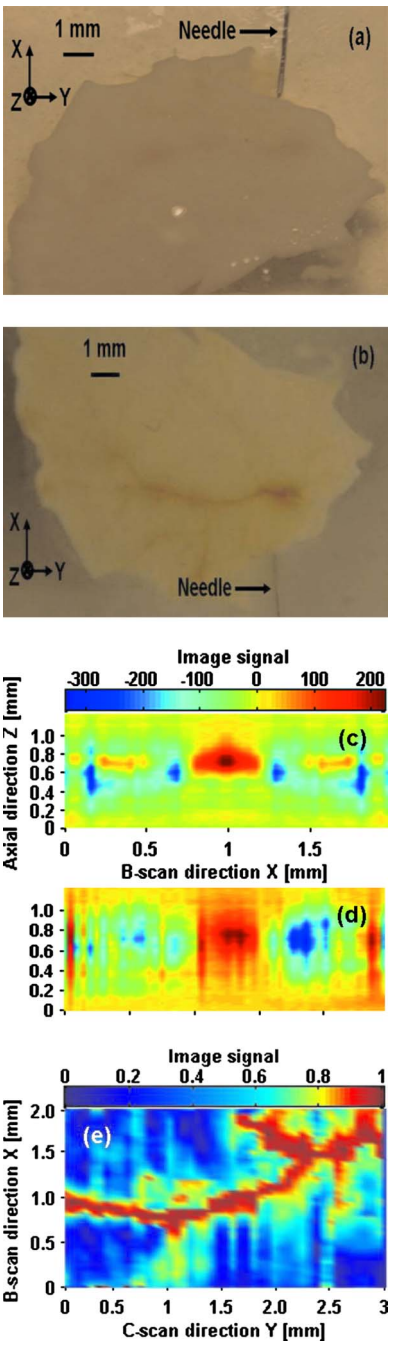

Fig. 4 Imaging blood vasculature with mouse skin intact. (a) Photograph of the exterior of the skin sample obtained from the mouse. (b) The vascular distribution intact with the skin sample photographed from the underside. (c) and (d) Two consecutive B-scan images that were obtained 0.2 mm apart laterally at y=1.5 mm and y=1.7 mm, respectively. (e) MIP image of (a) obtained using UOM.

we prepared an optically scattering sample and embedded three optically absorbing objects (μ_a=145 cm^{-1}, μ_a =72 cm^{-1}, and μ_a=36 cm^{-1}, with all three having the same μ_s'=0.5 cm^{-1}) and one nearly transparent object (μ_a =0.1 cm^{-1}, μ_s'=0.5 cm^{-1}), 3.0 mm below the surface of the sample. Photographs of the objects and the prepared phantom are shown in Figs. 2(a) and 2(b), respectively. Figure 2(c) shows a background subtracted 2-D (B-scan) image of all four

objects shown in Fig. 2(a), obtained by scanning the sample in the x direction. Respective 1-D profiles (A-lines) along the z axis through the center of all four objects are plotted in Fig. 2(d). Figures 2(c) and 2(d) demonstrate that the image contrasts of all three absorbing objects are negative, whereas the image contrast of the transparent object is positive. Further, the image contrast of all three absorbing objects decreases with a decrease in absorption coefficient.

Figure 2(e) presents normalized 1-D profiles (A-lines), acquired from the original data, along the z axis through the center of all four objects and the background medium BG. These A-lines represent the temporal dependence of the ultrasound modulated light intensity during ultrasound-pulse propagation through the sample. For each A-line, the time of propagation is multiplied by 1500 ms^{-1}, the approximate speed of sound in the sample, to be converted to distance along the z axis, where the origin of each A-line corresponds to the trigger for the signal acquisition from the APD. For the given acoustic parameters, these results demonstrate that the characteristics of the ultrasound-modulated optical signal were influenced by the size and the absorption coefficient of the object and by the scattering properties of the objects and surrounding medium. As shown in Fig. 2(e), both the width and height of the signal drop decrease with a decrease in the absorption coefficient of the object. This decrease in the width of the signal drop can be attributed to increased diffusion of photons (into the object) with a decrease in the absorption coefficient of the object. The decrease in the height of the signal drop with an increase in the absorption coefficient of the object can be directly related to an increase in the absorption of photons. In addition, the comparison between A-lines through the centers of the transparent object ($\mu_s'=0.5$ cm^{-1} and $\mu_a=0.1$ cm^{-1}) and the background medium ($\mu_s'=10$ cm^{-1} and $\mu_a=0.1$ cm^{-1}) shows that the shape of the ultrasound-modulated optical signal (A-line) is quite sensitive to the local (confined by the ultrasound focal volume) optical scattering properties relative to the scattering properties of the background medium. Figure 2(c) also shows that the intensity of modulated light passing through the transparent object is more than that through the background medium. Since the transparent object and the background have the same μ_a, this increase in the intensity and the change in the shape of the A-line passing through the center of the transparent object can be attributed to the lower μ_s' of the transparent object than that of the background.

We further measured the contrast at the center of all three absorbing objects in Fig. 2(c), and plotted the results in Fig. 2(f). This measurement demonstrates that the contrast of each object was nearly linearly related to the absorption coefficient of the object. Simple theoretical considerations show that at the limit, where the absorption length (reciprocal of the absorption coefficient) is small compared to the path length of the light through the absorbing object, the dependence of the ultrasound-modulated signal intensity on the object absorption is nearly linear.[33] More importantly, the measurable absorptions are clearly much lower than the blood absorption ($\mu_a=120$ cm^{-1} at 532-nm wavelength), which implies that this technology has great potential in detecting small blood vessels and other functional parameters associated with blood, such as oxygenation saturation.

3.2 *Ex Vivo Blood Vessel Imaging Using Tissue Samples*

3.2.1 *Imaging intact blood vasculature in a rat ear*

In this section we explore the potential of UOM for imaging intrinsic optical absorption due to blood, using ear and skin tissue samples obtained from a dead mouse and rat. As described in the phantom preparation section, these optically scattering tissue samples were placed in a clear medium. Figure 3(a) shows a photograph of blood vasculature inside the rat ear. Based on this photograph, the imaged vessels were $\sim$100 μm in diameter and the ear is about 350 μm thick. A piece of stainless steel needle (outer diameter 250 μm) was used to align the focal plane of the ultrasound transducer with the plane of the ear placed inside a 5-mm-thick clear medium. Figure 3(b) shows a typical normalized A-line (A-1) from the original data, passing through the blood vessel located about 300 μm deep in the ear tissue sample. A dot placed below this represents the position of the blood vessel along the ultrasound propagation direction (axial direction or depth direction). The local drop in the signal strength at the position of the blood vessel is primarily due to ultrasound-modulated optical absorption of blood. A-2 represents the A-line not passing through the blood vessel. Figures 3(c)–3(f) show four consecutive UOM B-scan images that were obtained 0.2 mm apart laterally at $y=0.2$ mm, $y=0.4$ mm, $y=0.6$ mm, and $y=0.8$ mm, respectively. These images are obtained by subtracting each A-line in one B-scan from the first A-line during the respective B-scan acquisition. As discussed in the previous sections, a B-scan image is a 2-D cross-sectional image (along the x-z plane) obtained by scanning the sample along the x direction and acquiring each corresponding 1-D image (A-line) with identical y coordinates. Each B-scan took about 8 min to complete (100 A-lines, 20-μm step size, and 5-s/A-line). The vertical axis of the B-scan image represents the depth from the surface of the ear, and the horizontal axis represents the position of the transducer along the x (B-scan) direction. Encircled regions in Fig. 3(c) show the typical cross section of the blood vessel, perpendicular to the imaging plane, which is nearly circular. The vessel is $\sim$0.1 mm in diameter in the image. In Fig. 3(c), the typical image contrast-to-noise ratio of blood with respect to background skin tissue is about 6:1. In Fig. 3(b), A-1 presents an 80% drop in the signal at the position of the blood vessel. With reference to our discussion in Fig. 2, we can infer that this drop translates to an 80% image contrast between blood and background tissue. From these B-scan images [also from the results on absorbing objects in Fig. 2(e)], we can infer that UOM has the potential to image the interior of blood vessels. After each B-scan along the x axis, the sample was returned to its original x coordinate and further translated by one scanning step (0.1 mm) along the y axis to start a new B-scan. Thus, by raster scanning the sample in the x-y plane, we obtained a total of 10 B-scans.

To obtain high contrast blood vessel imaging, each B-scan was processed by subtracting each A-line in the B-scan from an A-line obtained from the transparent region of the respective B-scan. We further performed maximum intensity projection (MIP) along the z axis on each of the processed B-scan images. The final MIP image, Fig. 3(f), was obtained by com-

bining projections from all B-scans. The blood vessel structure in the projection image, Fig. 3(g), is in agreement with the photograph [Fig. 3(a)].

3.2.2 *Imaging intact blood vasculature in mouse skin*

Figure 4(a) shows a photograph of the exterior of the skin sample obtained from the mouse. Figure 4(b) shows the vascular distribution intact with the skin sample photographed from the underside. As discussed in the previous section, the tissue sample was raster scanned in the x-y plane. Each B-scan took about 4 min (50 A-lines, 40-μm step size, and 5-s/A-line). We obtained a total of 30 B-scans by translating the sample along the y axis with a step size of 0.1 mm. Each A-line in one B-scan is subtracted from the first A-line during the respective B-scan acquisition. Figures 4(c) and 4(d) show B-scan images at $y=1.5$-mm and $y=1.7$-mm positions in the MIP image [Fig. 4(e)] of Fig. 4(a), respectively. In Fig. 4(c), the typical image contrast-to-noise ratio of blood with respect to background skin tissue is about 4:1. The vessel is $\sim$0.1 mm in diameter in the image. Good agreement in the vascular structure can be observed between the projected image [Fig. 4(e)] and the photograph [Fig. 4(a)].

4 Conclusions

In summary, this study demonstrates the feasibility of blood vasculature imaging using ultrasound-modulated optical microscopy, and suggests the potential for functional imaging of living subjects. The high image contrast of the blood vasculature in our results is primarily due to the ultrasound-modulated optical absorption of blood in tissue samples. We also demonstrate that UOM is sensitive to both optical absorption and scattering contrast. For the given acoustic parameters, these results demonstrate that the shape, height (strength), and width of the ultrasound-modulated optical signal are influenced by the size and the absorption coefficient of the object, and by the scattering properties of the objects and surrounding medium.

Acknowledgment

This research was supported by the National Institutes of Health grants R33 CA094267 and R01 CA106728.

References

1. T. F. Massoud and S. S. Gambhir, "Molecular imaging in living subjects: seeing fundamental biological processes in a new light," *Genes Dev.* **17**, 545–580 (2003).
2. H. Gurden, N. Uchida, and Z. Mainen, "Sensory-evoked intrinsic optical signals in the olfactory bulb are coupled to glutamate release and uptake," *Neuron* **52**, 335–345 (2006).
3. P. G. Aitken, D. Fayuk, G. G. Somjen, and D. A. Turner, "Use of intrinsic optical signals to monitor physiological changes in brain tissue slices," *Methods* **18**, 91–103 (1999).
4. R. Weissleder and V. Ntziachristos, "Shedding light onto live molecular targets," *Nat. Med.* **9**, 123–128 (2003).
5. H. F. Zhang, K. Maslov, G. Stoica, and L. H. Wang, "Functional photoacoustic microscopy for high-resolution and noninvasive in vivo imaging," *Nat. Biotechnol.* **24**, 848–851 (2006).
6. J. G. Fujimoto, "Optical coherence tomography for ultrahigh resolution *in vivo* imaging," *Nat. Biotechnol.* **21**, 1361–1367 (2003).
7. H. Inoue, S. Kudo, and A. Shiokawa, "Laser-scanning confocal microscopy and endocytoscopy for cellular observation of the gastrointestinal tract," *Nat. Clin. Pract. Gastroenterol. Hepatol.* **2**, 31–37 (2005).
8. S. Srinivasan, B. W. Pogue, S. Jiang, H. Dehghani, C. Kogel, S. Soho, J. J. Gibson, T. D. Tosteson, S. P. Poplack, and K. D. Paulsen, "Interpreting hemoglobin and water concentration, oxygen saturation and scattering measured in vivo by near-infrared breast tomography," *Proc. Natl. Acad. Sci. U.S.A.* **100**, 12349–12354 (2003).
9. L. V. Wang and H. I. Wu, *Biomedical Optics: Principles and Imaging*, Wiley, New York (2007).
10. A. A. Oraevsky, E. V. Savateeva, S. V. Solomatin, A. A. Karahutov, V. G. Andreev, Z. Gatalica, and T. Khamapirad, "Optoacoustic imaging of blood for visualization and diagnostics of breast cancer," *Proc. SPIE* **4618**, 81–94 (2002).
11. S. Leveque, A. C. Boccara, M. Lebec, and H. Saint-Jalmes, "Ultrasonic tagging of photon paths in scattering media: parallel speckle modulation processing," *Opt. Lett.* **24**, 181–183 (1999).
12. A. D. Aguirre, Y. Chen, J. G. Fujimoto, L. Ruvinskaya, A. Devor, and D. A. Boas, "Depth-resolved imaging of functional activation in the rat cerebral cortex using optical coherence tomography," *Opt. Lett.* **31**, 3459–3461 (2006).
13. L. V. Wang, "Ultrasound-mediated biophotonic imaging: a review of acousto-optical tomography and photo-acoustic tomography," *Dis. Markers* **19**, 123–138 (2004).
14. S. R. Kothapalli, S. Sakadzic, C. Kim, and L. V. Wang, "Imaging optically scattering objects with ultrasound-modulated optical tomography," *Opt. Lett.* **32**, 2351–2353 (2007).
15. X. Xu, H. Zhang, D. Qing, C. Kim, P. Hemmer, and L. V. Wang, "Photorefractive detection of tissue optical and mechanical properties by ultrasound modulated optical tomography," *Opt. Lett.* **32**, 656–658 (2007).
16. W. Leutz and G. Maret, "Ultrasonic modulation of multiply scattered-light," *Physica B* **204**, 14–19 (1995).
17. L. V. Wang, "Mechanisms of ultrasonic modulation of multiply scattered coherent light: an analytic model," *Phys. Rev. Lett.* **87**, 043903 (2001).
18. S. Sakadzic and L. V. Wang, "Modulation of multiply scattered coherent light by ultrasonic pulses: Analytical model," *Phys. Rev. E* **72**, 036620 (2005).
19. S. Sakadžić and L. V. Wang, "Correlation transfer and diffusion of ultrasound-modulated multiply scattered light," *Phys. Rev. Lett.* **96**, 163902 (2006).
20. L. V. Wang and G. Ku, "Frequency-swept ultrasound-modulated optical tomography of scattering media," *Opt. Lett.* **23**, 975–977 (1998).
21. G. Yao, S. L. Jiao, and L. V. Wang, "Frequency-swept ultrasound-modulated optical tomography in biological tissue by use of parallel detection," *Opt. Lett.* **25**, 734–736 (2000).
22. M. Hisaka, T. Sugiura, and S. Kawata, "Optical cross-sectional imaging with pulse ultrasound wave assistance," *J. Opt. Soc. Am. A Opt. Image Sci. Vis* **18**, 1531–1534 (2001).
23. J. Li, G. Ku, and L. V. Wang, "Ultrasound-modulated optical tomography of biological tissue by use of contrast of laser speckles," *Appl. Opt.* **41**, 6030–6035 (2002).
24. A. Lev and B. G. Sfez, "Pulsed ultrasound-modulated light tomography," *Opt. Lett.* **28**, 1549–1551 (2003).
25. T. W. Murray, L. Sui, G. Maguluri, R. A. Roy, A. Nieva, F. Blonigen, and C. A. DiMarzio, "Detection of ultrasound modulated photons in diffuse media using the photorefractive effect," *Opt. Lett.* **29**, 2509–2511 (2004).
26. S. Sakadzic and L. V. Wang, "High-resolution ultrasound-modulated optical tomography in biological tissues," *Opt. Lett.* **29**, 2770–2772 (2004).
27. Y. Li, H. Zhang, C. Kim, K. H. Wagner, P. Hemmer, and L. V. Wang, "Pulsed ultrasound-modulated optical tomography using spectral-hole burning as a narrowband spectral filter," *Appl. Phys. Lett.* **93**, 011111-(1–3) (2008).
28. G. Rousseau, A. Blouin, and J. Monchalin, "Ultrasound-modulated optical imaging using a powerful long pulse laser," *Opt. Express* **16**, 12577–12590 (2008).
29. S. R. Kothapalli and L. V. Wang, "Ultrasound-modulated optical microscopy," *J. Biomed. Opt.* **13**, 0504046-(1–8) (2008).
30. J. W. Wallis, T. R. Miller, C. A. Lerner, and E. C. Kleerup, "Three-dimensional display in nuclear medicine," *IEEE Trans. Med. Imaging* **8**, 297–303 (1989).
31. F. A. Duck, "Medical and non-medical protection standards for ultrasound and infrasound," *Prog. Biophys. Mol. Biol.* **93**, 176–191 (2007).
32. Laser Institute of America, *American National Standard for the Safe Use of Lasers ANSI Z136.1-2000*, ANSI, Orlando, FL (2000).
33. G. Yao and L. V. Wang, "Signal dependence and noise source in ultrasound-modulated optical tomography," *Appl. Opt.* **43**, 1320–1326 (2004).